MPC for Vehicle Lateral Stability Via Differential Braking and Active Front Steering Considering Practical Aspects

Mooryong Choi[1] and Seibum B. Choi[2]

Abstract
This paper presents a control architecture that simultaneously utilizes active front steering (AFS) and differential braking for vehicle lateral stability while minimizing longitudinal perturbations. This control scheme is based on the model predictive control (MPC) using the extended bicycle model that captures the lagged characteristics of tire forces and actuators. The nonlinearities of tire force are also reflected on the extended bicycle model by linearizing the tire forces at the operating points. Instead of casting the MPC problem into a quadratic program with constraints that require numerical solvers, the proposed method is designed to follow the reference states with desired inputs since the solutions of MPC problems with affine models to track desired states can be easily obtained by matrix inversion. Simulation results, obtained by the vehicle dynamics software CarSim, demonstrate that the suggested method is able to control the vehicle to track the desired path while keeping the vehicle lateral stability on various road surfaces.

Nomenclature

β	Vehicle side slip angle
δ_f	Average front steer angle
μ	Tire-road friction coefficient
C_α	Tire lateral stiffness parameter
C_f	Lumped cornering stiffness of front tires
C_r	Lumped cornering stiffness of rear tires
C_x	Tire longitudinal stiffness parameter
F_x	Tire longitudinal force
F_z	Tire normal force
F_{yf}	Front axle lateral tire force
F_{yr}	Rear axle lateral tire force
I_z	Vehicle yaw moment of inertia
l_f	CG-front axle distance
l_r	CG-rear axle distance
m	Vehicle mass
M_z	Corrective yaw moment
N	Prediction horizon
P_B	Brake cylinder pressure of each wheel
r	Vehicle yaw rate
R_e	Tire effective radius
t	Vehicle half track
v_x	Vehicle longitudinal speed
v_y	Vehicle lateral speed

Introduction

To correspond with the increased demand for vehicle safety, various types of vehicle safety systems have penetrated into the automotive market over the last two decades (1; 2; 5; 6; 7; 8; 9; 10; 11; 12; 13; 14). Among them, electronic stability control (ESC) has proven itself as one of the most effective systems that enhance vehicle safety (15). Consequently, the U.S. government has recently obligated all new passenger vehicles sold in the United States to be equipped with the ESC. The ESCs stabilize the vehicle yaw motions by actuating the differential brakings at the cost of undesirable longitudinal perturbations. Active front steering (AFS) systems, which are also promising vehicle safety systems, have started to be adopted for some passenger vehicles (16). AFS can modify the front tire road wheel angle independent of the steering wheel angle to achieve improved cornering performance and vehicle yaw stability. Although, AFSs are less effective in stabilizing the vehicles at the limits of handling comparing to ESCs, they have advantages in the

[1]R&D Division, Hyundai-Kia Motor Group
[2]Department of Mechanical Engineering, KAIST (Korea Advanced Institute of Science and Technology)

Corresponding author:
Seibum B. Choi, Department of Mechanical Engineering, KAIST, Daejeon 305-701, Korea
Email: sbchoi@kaist.ac.kr

fact that they do not perturb vehicle longitudinal dynamics unlike ESCs.

As a result, because of the potential characteristic of AFS that can assist ESC to minimize the longitudinal perturbation to stabilize the vehicles at the limits of handling, a wide range of studies that coordinates AFS and ESC to secure the vehicle yaw stability has been introduced in the literature (16; 3; 4). Although the performances of these algorithms are satisfactory according to their simulations or experimental results, they do not appropriately account for the deteriorations of the performances caused by the lags of actuators of AFSs or ESCs. Since a vehicle in an unstable state region can rapidly deviate from its desired trajectory, even in a short time, small delays or lags of the vehicle safety systems can lead to fatal vehicle accidents. Model predictive control (MPC) can be a good candidate to deal with these actuation lags because the predictive characteristics of MPC enable earlier actuations to compensate for the lags of the actuators. There have been several attempts to apply MPC to ESC, AFS or coordinating ESC and AFS (17; 18; 19; 20; 21; 22). However, these attempts focus only on minimizing required inputs using predictive characteristics of MPC or capabilities of MPC that can effectively process multiple input and output systems. The vehicle models used for prediction of these MPC algorithms do not appropriately reflect actuation lags. Therefore, in this paper, a method to stabilize a vehicle that fully utilizes the predictive characteristics of MPC by employing the vehicle model that captures the lags of tire forces and actuators for ESC and AFS is presented.

Furthermore, unlike MPC-based methods presented in (17; 18; 19; 20; 21; 22), the method to be presented is designed not to cause a huge computational burden, which is the primary issue that remains unsolved in commercializing these MPC-based yaw stability algorithms. This computational burden mostly originates from the nonlinearities of the vehicle models and inequality constraints to limit the states of the vehicle model in certain bounds in the MPC problem. To avoid these issues, the nonlinear characteristics of tire forces, such as the friction ellipse effect or the tire force saturation, are taken into account by linearizing the tire forces about their operating points while designing the extended bicycle, which is used as the prediction model of MPC problem.

To remove the inequality constraints for the state of the bicycle model, the MPC is designed to track the desired states instead of restraining them by inequality constraints. Since the extended bicycle model is linear, the cost function for the MPC problem can be expressed as a quadratic function with equality constraints. The optimal solution of this MPC problem can be easily obtained by matrix inversion without using complicated numeric solvers.

The computational burden also grows exponentially as the number of input variables increases. To reduce the number of input variables, the upper controller based on the MPC problem calculates the required corrective yaw moment only. The coordinator determines the values of the modified steer angle of AFS and brake pressures of individual wheels to recreate the calculated corrective yaw moment from the supervisor based on a rule-based algorithm and an optimization problem.
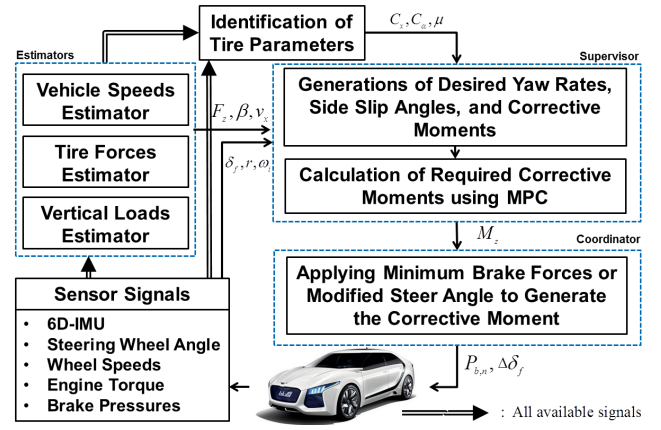

Figure 1. Flow structure of the entire control system.

Overall Control Architecture

In this section, the overall control architecture and its intrinsic modular structures to stabilize vehicle lateral motion are demonstrated. Figure 1 shows the flow structure of the proposed MPC-based controller which consists of the supervisor and the coordinator with the estimators and the sensor signals. By making full use of the readily available sensor signals of commercial vehicles equipped with AFSs and ESCs, including δ_{fs}, the steer angle from the driver's input, $\Delta\delta_f$, the modified steer angle by AFS, ω_i, the wheel speeds, T_e, the engine torque, $P_{b,i}$, the brake pressures, a_x, the longitudinal acceleration, a_y, the lateral acceleration, and r, yaw rate, the estimators are designed to observe v_x, the vehicle longitudinal speed, v_y, vehicle lateral speed, $F_{x,i}$, longitudinal tire force, F_{yf}, front axle lateral tire force, F_{yr}, rear axle lateral tire force, and $F_{z,i}$, vertical load where $i = 1, 2, 3, 4$ which correspond to the left-front, right-front, left-rear, and right-rear wheels, respectively. The tire parameter identifier and the main controller simultaneously operate employing these estimated values. In the tire parameter identifier, the values of C_x, which is the tire longitudinal stiffness parameter, C_α, which is the tire lateral stiffness parameter, and μ, which is the tire-road friction coefficient are identified by the linearized recursive least square method with the estimated values of v_x, v_y, $F_{x,i}$, F_{yf}, F_{yr}, and $F_{z,i}$. The supervisor as an upper-level controller calculates the corrective yaw moment M_z to be exerted on the vehicle after receiving information about the vehicle state and the tire parameters. Then, the coordinator optimally distributes required $P_{B,i}$ and $\Delta\delta_f$ to recreate the calculated M_z from the supervisor. For more details about the above estimators and the tire parameter identifier, (23) and (24) can be referred to, respectively.

Vehicle Models

For the supervisor whose main algorithm relies on the MPC scheme, two linear vehicle models are required: the linear bicycle model for generating the desired yaw rate and the bicycle model based on linearized tire forces for predicting the future vehicle behavior. These two vehicle models that are integrated with the dynamic tire model (26) and the actuator models expressed as first-order lag functions are
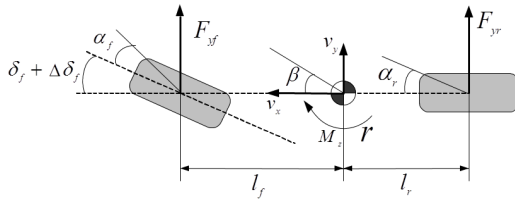
Figure 2. Schematic of vehicle lateral dynamic model.

developed to capture the lagged characteristics of tire forces and actuators in the vehicle models.

Bicycle Model with Lagged Dynamics

The bicycle model is a dynamic model which describes the vehicle lateral dynamics as shown in Fig. 2. The equations for the vehicle lateral dynamics can be expressed as follows:

$$mv_x(\dot{\beta} + r) = F_{yf} + F_{yr} \tag{1}$$
$$I_z\dot{r} = l_f F_{yf} - l_r F_{yr} + M_z, \tag{2}$$

where I_z and m are the vehicle yaw moment of inertia and the mass, respectively. In (1) and (2), F_{yf} and F_{yr} are simplified with the linear tire models as follows:

$$F_{yf} = C_f \alpha_f \tag{3}$$
$$F_{yr} = C_r \alpha_r, \tag{4}$$

where

$$\alpha_f = \delta_f - \left(\beta + \frac{l_f \cdot r}{v_x}\right) \tag{5}$$
$$\alpha_r = -\beta + \frac{l_r \cdot r}{v_x}, \tag{6}$$

with

$$\delta_f = \delta_{fs} + \Delta\delta_f.$$

In (3) and (4), α_f and α_r are the slip angles of the front and rear tires while C_f and C_r indicate the front and rear cornering stiffnesses, respectively. v_x is assumed to be a constant for a short period of time.

The dynamic tire model developed with first order lag function in (26) can be expressed as follows:

$$\tau_l \dot{F}_{yf\_lag} + F_{yf\_lag} = F_{yf} \tag{7}$$
$$\tau_l \dot{F}_{yr\_lag} + F_{yr\_lag} = F_{yr}, \tag{8}$$

where F_{yf_lag} and F_{yr_lag} are the lagged lateral tire force of the front and rear tires, respectively. τ_l is the relaxation time constant defined as

$$\tau_l = \frac{C_\alpha}{K_e v_x}, \tag{9}$$

where K_e is the equivalent tire lateral stiffness (26).

The actuators of ESC and AFS, which are hydraulic brake system and electric motor, respectively, can also be simply expressed as a first-order lag function (26). Since M_z in (2) to be exerted to the vehicle is recreated by these actuators,

the lag function of M_z can be modeled as follows:

$$\tau_* \dot{M}_{z\_lag} + M_{z\_lag} = M_z. \tag{10}$$

M_{z_lag} is the lagged corrective yaw moment. τ_* stands for τ_b, the time constant of the hydraulic brake model, when differential braking is applied or τ_s, the time constant of the actuator model for AFS, when AFS is activated. By taking Laplace transforms, the lagged tire forces and the corrective moment in Laplace domain can be presented as follows:

$$F_{yf\_lag}(s) = \frac{C_f \alpha_f(s)}{\tau_l s + 1} \tag{11}$$

$$F_{yr\_lag}(s) = \frac{C_r \alpha_r(s)}{\tau_l s + 1} \tag{12}$$

$$M_{z\_lag}(s) = \frac{M_z}{\tau_* s + 1}. \tag{13}$$

By replacing F_{yf}, F_{yr}, and M_z with F_{yf_lag}, F_{yr_lag}, and M_{z_lag} respectively, (1) and (2) can be rewritten as follows:

$$mv_x(\dot{\beta} + r) = F_{yf\_lag} + F_{yr\_lag} \tag{14}$$
$$I_z\dot{r} = l_f F_{yf\_lag} - l_r F_{yr\_lag} + M_{z\_lag}. \tag{15}$$

By substituting (11)-(13), (14) and (15) can be reexpressed in Laplace domain as follows:

$$mv_x(\tau_l s^2 \beta + s\beta + r) = C_f \alpha_f(s) + C_r \alpha_r(s) \tag{16}$$
$$I_z(\tau_* \tau_l s^3 r + (\tau_* + \tau_l)s^2 r + sr) \tag{17}$$
$$= (\tau_* s + 1)l_f C_f \alpha_f(s) + (\tau_* s + 1)l_r C_r \alpha_r(s) + (\tau_l s + 1)M_z(s).$$

By taking the inverse Laplace transform and rearranging the terms, (16) and (17) can be augmented in a state-space form:

$$\dot{x} = A_l x + B_{l,\delta}\begin{bmatrix} \delta_f \\ \dot{\delta}_f \end{bmatrix} + B_M\begin{bmatrix} M_z \\ \dot{M}_z \end{bmatrix}, \tag{18}$$

where

$$x = \begin{bmatrix} \beta & \dot{\beta} & r & \dot{r} & \ddot{r} \end{bmatrix}^T \tag{19}$$

and A_l, $B_{l,\delta}$, and B_M are defined in (20).

Tire Model

The bicycle model with the lagged dynamics (18) is valid only when the lateral tire forces show linear characteristics since the model is built based on the linear tire models expressed in (3) and (4). However, AFS and ESCs are most commonly activated when nonlinear characteristics of tire forces, such as the friction ellipse effect or tire force saturation, appear since vehicles tend to loose lateral stability when the tires generate lateral forces close to their frictional limits.

Therefore, the following longitudinal and lateral combined brushed tire model (26; 27) that can adequately describe the tires' nonlinear characteristics is adopted to develop the supervisor controller.

$$F_{x,i} = \frac{C_x\left(\frac{\kappa_i}{1+\kappa_i}\right)}{f_i}F_i \tag{21}$$

$$A_l = \begin{bmatrix} 0 & 1 & 0 & 0 & 0 \\ -\frac{C_f+C_r}{\tau_l m V_x} & -\frac{1}{\tau_l} & \left(\frac{C_r l_r - C_f l_f}{\tau_l m V_x^2} - \frac{1}{\tau_l}\right) & -1 & 0 \\ 0 & 0 & 0 & 1 & 0 \\ 0 & 0 & 0 & 0 & 1 \\ \frac{C_r l_r - C_f l_f}{\tau_* \tau_l I_z} & \frac{C_r l_r - C_f l_f}{\tau_l I_z} & -\frac{C_f l_f^2 + C_r l_r^2}{\tau_* \tau_l I_z V_x} & -\frac{C_f l_f^2 + C_r l_r^2}{\tau_l I_z V_x} - \frac{1}{\tau_* \tau_l} & -\frac{\tau_* + \tau_l}{\tau_* \tau_l} \end{bmatrix}$$

(20)

$$B_{l,\delta} = \begin{bmatrix} 0 & 0 \\ \frac{C_f}{\tau_l m V_x} & 0 \\ 0 & 0 \\ 0 & 0 \\ \frac{C_f l_f}{\tau_l \tau_* I_z} & \frac{C_f l_f}{\tau_l I_z} \end{bmatrix}, \quad B_M = \begin{bmatrix} 0 & 0 \\ 0 & 0 \\ 0 & 0 \\ 0 & 0 \\ \frac{1}{\tau_l \tau_* I_z} & \frac{1}{\tau_l I_z} \end{bmatrix}$$
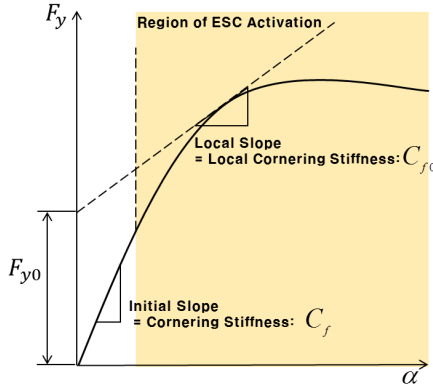

Figure 3. Linearization of tire force

$$F_{y,i} = -\frac{C_\alpha \left(\frac{\tan \alpha_i}{1+\kappa_i}\right)}{f_i} F_i,$$

(22)

where

$$F_i = \begin{cases} f_i - \frac{1}{3\mu F_{z,i}} f_i^2 + \frac{1}{27\mu^2 F_{z,i}^2} f_i^3 & \text{if } f_i \le 3\mu F_{z,i} \\ \mu F_{z,i} & \text{else} \end{cases}$$

$$f_i = \sqrt{C_x^2 \left(\frac{\kappa_i}{1+\kappa_i}\right)^2 + C_\alpha^2 \left(\frac{\tan \alpha_i}{1+\kappa_i}\right)^2}$$

$$\kappa_i = \frac{R_{e,i}\omega_i - v_{xt,i}}{v_{xt,i}}$$

(23)

$$\begin{bmatrix} \alpha_1 \\ \alpha_2 \\ \alpha_3 \\ \alpha_4 \end{bmatrix} = \begin{bmatrix} \delta_f \\ \delta_f \\ 0 \\ 0 \end{bmatrix} - \tan^{-1} \begin{bmatrix} \frac{v_y + l_f r}{v_x} \\ \frac{v_y + l_f r}{v_x} \\ \frac{v_y - l_r r}{v_x} \\ \frac{v_y - l_r r}{v_x} \end{bmatrix}.$$

(24)

In (21) and (22), κ_i and α_i respectively denote the slip ratio and the slip angle of the ith wheel as defined in (23) and (24), ω_i the wheel speed, R_e the effective radius, and $v_{t,i}$ the speed of a vehicle at the tire position.

Bicycle Model with Linearized Tire Forces

As explained in the previous section, when vehicles loose their lateral stabilities at the limit of handling, adequate lateral tire forces are not generated due to their tire force saturations. When ESC or AFS is activated to stabilize the vehicle, it is most likely that tire forces show nonlinear characteristics.

However, the linear bicycle model (18) is valid only when the lateral tire forces show linearities as the slip angles increase. To extend the usage of the linear bicycle model (18) to the case when tire forces grow nonlinearly along with increasing slip angles, the linear tire models (3) and (4) that are used to construct the bicycle model (18) are newly defined as follows:

$$F_{yf} = C_{f0}\alpha_f + F_{yf0}$$

(25)

$$F_{yr} = C_{r0}\alpha_r + F_{yr0}.$$

(26)

These models are obtained by linearizing the longitudinal and lateral combined brushed tire model (21) and (22) at the current $F_{z,i}$, α_i, and κ_i. In (25) and (26), C_{f0} and C_{r0} denote the gradients of the lateral tire curves at the current linearizing points while F_{yf0} and F_{yr0} indicate the residual lateral forces, as depicted in Fig.3.

Since the parameters of tire model (21) and (22), i.e., C_x, C_α, and μ are identified in real time using the method introduced in (24), the values of C_{f0}, C_{r0}, F_{yf0}, and F_{r0} are updated at each time step to reflect the change of surface conditions and the nonlinear characteristics of tire forces while operating the suggested controller.

Instead of (3) and (4), (25) and (26) are substituted into (7) and (8). Due to the additional terms, F_{yf0} and F_{r0} in (25) and (26), E_{add} is added to (18) and reexpressed as follows:

$$\dot{x} = Ax + B_\delta \begin{bmatrix} \delta_f \\ \dot{\delta}_f \end{bmatrix} + B_M \begin{bmatrix} M_z \\ \dot{M}_z \end{bmatrix} + E_{add},$$

(27)

where

$$E_{add} = \begin{bmatrix} 0 & \frac{F_{0f} + F_{0r}}{\tau_l m v_x} & 0 & 0 & \frac{l_f F_{0f} - l_r F_{0r}}{\tau_l \tau_* I_z} \end{bmatrix}^T.$$

A and B_δ are obtained from A_l and $B_{l,\delta}$ after replacing C_f and C_r in A_l and $B_{l,\delta}$ by C_{f0} and C_{r0}, respectively.

Development of Supervisor

In the previous sections, the vehicle models that are required to form the MPC problem were developed. In this section, utilizing these vehicle models, the MPC problem that can

generate the optimal corrective yaw moment to be applied to the vehicle to track reference states is illustrated. The methods of generating the reference states and coordinating AFS and ESC which are dependent on a rule-based algorithm, are also presented.

MPC Formulation

A model predictive controller finds a set of optimal inputs, that minimize the cost function while satisfying input constraints over a specified prediction time horizon, and apply only the first input in the sequence of the optimal inputs to the system at each time step. First, to form an MPC problem, the bicycle model with linearized tire forces (27) is discretized using a zero-order hold as follows:

$$x_{k+1} = A_d x_k + B_{M,d} \begin{bmatrix} u_k \\ \frac{u_k - u_{k-1}}{t_s} \end{bmatrix} + E_k, \qquad (28)$$

where

$$E_k = B_{\delta,k} \begin{bmatrix} \delta_f + t_s \cdot k \cdot \dot{\delta}_f \\ \dot{\delta}_f \end{bmatrix} + E_{add,d}, \quad u_k = M_{z,k}.$$

The subscript d denotes that the correspond time-invariant matrices are discretized and k denotes that the corresponding discretized matrices are at the kth step in discrete time. The terms in E_k, including δ_f, are set to be constants for the prediction time span while developing (28). The cost function of MPC with equality constraints in a quadratic form is defined as follows:

$$J(x(0),U) = \sum_{k=0}^{N-1} (x_k - x_{r,k})^T Q(x_k - x_{r,k}) \cdots \qquad (29)$$
$$+ (u_k - u_{r,k})^T R(u_k - u_{r,k}) + (x_N - x_{r,N})^T P(x_N - x_{r,N})$$

$$\text{subj. to } x_{k+1} = A_d x_k + B_{M,d} \begin{bmatrix} u_k \\ \frac{u_k - u_{k-1}}{t_s} \end{bmatrix} + E_k, \qquad (30)$$

where

$$U = [u_0, \dots u_{N-1}]'$$

with Q, P, and R, which are the weighting matrices with corresponding dimensions. x_r and u_r refer to the reference state and the reference corrective yaw moment, respectively. The method of generating x_r and u_r are to be presented in the next subsections.

Closed Form Solution for MPC

Since the bicycle model (18) with the linearized tire model is linear, inequality constraints in the quadratic cost function (29) are omitted, and the MPC controller is designed for the vehicle to follow the reference states with the reference inputs, the closed form solution of the MPC problem can be acquired without using numerical solvers. The terms with constant values, which do not affect the value of the optimal solution, can be removed from (29) and it can be rewritten as

$$J(x(0),U) = \sum_{k=0}^{N-1} x_k' Q x_k - 2x_{r,k}{}^T Q x_k - x_k{}^T Q x_{r,k} \cdots$$
$$+ u_k{}^T R u_k - 2u_{r,k}{}^T R u_k + x_N{}^T P x_N - 2x_{r,N}{}^T P x_N. \qquad (31)$$

The equality constraints in (30) can be explicitly rewritten with all future states $x_1, x_2, \dots x_N$ and the future inputs $u_0, u_1, \dots u_{N-1}$:

$$\underbrace{\begin{bmatrix} x(0) \\ x_1 \\ \vdots \\ \vdots \\ x_N \end{bmatrix}}_{X} = \underbrace{\begin{bmatrix} I \\ A_d \\ \vdots \\ \vdots \\ A_d^N \end{bmatrix}}_{S^x} x(0) \cdots \qquad (32)$$

$$+ \underbrace{\begin{bmatrix} 0 & & \dots & \dots & 0 \\ B_1 & 0 & \dots & & 0 \\ [A_d B_1 + B_2] & \ddots & \ddots & & \vdots \\ \vdots & & \ddots & \ddots & \vdots \\ A_d^{N-2}[AB_1 + B_2] & \dots & \dots & & B_1 \end{bmatrix}}_{S^u} \underbrace{\begin{bmatrix} u_0 \\ \vdots \\ \vdots \\ u_{N-1} \end{bmatrix}}_{U}$$

$$\cdots + \underbrace{\begin{bmatrix} 0 \\ E_1 \\ A_d E_1 + E_2 \\ \vdots \\ A_d^{N-1} E_1 + \dots + E_{N-1} \end{bmatrix}}_{S^e},$$

where

$$B_1 = B_{M1} + \frac{B_{M2}}{t_s}$$
$$B_2 = -\frac{B_{M2}}{t_s}$$
$$B_{M,d} = \begin{bmatrix} B_{M1} & B_{M2} \end{bmatrix}.$$

Since all future states are explicit functions of the present state $x(0)$ and the future and current inputs, $u_0, u_1, \dots u_{N-1}$, (32) can be expressed as follows:

$$X = S^x x(0) + S^u U + S^e. \qquad (33)$$

Using X as shown in (32), the cost function (31) can be rewritten as follows:

$$J(x(0),U) = X' \bar{Q} X + U' \bar{R} U + TX + T_u, \qquad (34)$$

where

$$\bar{R} = \text{blockdiag}\{R, \dots, R\}$$
$$\bar{Q} = \text{blockdiag}\{Q, \dots, Q, P\}$$
$$T = -2X_r' \bar{Q}$$
$$T_u = -2U_r' \bar{R}$$

with

$$X_r = [x_{r,0}, \dots x_{r,N}]^T$$
$$U_r = [u_{r,0}, \dots u_{r,N-1}]^T$$

By substituting (33) into (34), the cost function (34) can be rewritten as follows:

$$J(x(0),U) = (S^x x(0) + S^u U + S^e)^T \bar{Q}(S^x x(0) + S^u U + S^e) \cdots + U^T \bar{R} U + T(S^x x(0) + S^u U + S^e) + T_u. \qquad (35)$$

By dropping the terms with constant values and rearranging, the cost function (35) can be modified:

$$J(x(0), U) = U^T(S^{uT}\bar{Q}S^u + \bar{R})U \cdots \\ + [2x(0)^T(S^{xT}\bar{Q}S^u) + 2S^{eT}\bar{Q}S^u + TS^u + T_u]U. \quad (36)$$

Since (36) has a form of positive definite quadratic function of U, its minimum can easily be obtained by differentiating (36) with respect to U and finding U^* that set it to zero. The optimal inputs U^* with the given and the reference states are obtained as follows:

$$U^*(x(0), T, T_u) = -\tfrac{1}{2}(S^{uT}\bar{Q}S^u + \bar{R})^{-1}[2x(0)^T(S^{xT}\bar{Q}S^u)\cdots \\ + 2S^{eT}\bar{Q}S^u + TS^u + T_u]^T. \quad (37)$$

The MPC scheme finds the optimal solution U^* at each time step. However, only the current step input is utilized, and the remaining future inputs are discarded. The corrective yaw moment is applied to the vehicle by allocating differential brake forces to the wheels and modifying the front steer angle with AFS. The method of allocating differential brake forces and modifying the front steer angle for the given corrective yaw moment is introduced in the next section.

Generation of Reference Yaw Rates

The generation of reference yaw rates that the vehicle is to track is carefully carried out since the reference yaw rates have to reflect the driver's intention without exceeding the physical limits of the vehicle on a given surface. The N, the prediction horizon, number of reference yaw rates are generated using the bicycle model (18) with the following inputs:

$$\delta_{f,k} = \delta_f(0) + k \cdot t_s \cdot \dot{\delta}_f(0)$$
$$\dot{\delta}_{f,k} = \dot{\delta}_f(0)$$
$$M_{z,k} = 0.$$

However, since the bicycle model (18) does not reflect the physical limits of the tire forces, the absolute values of the reference yaw rates need to be truncated by appropriate upper bounds. The absolute values of the reference yaw rates have to satisfy the following inequality condition:

$$|r_{r,n}| \leq \left| \frac{(F_{yf\_\max} + F_{yr\_\max})}{mv_x} \right|, \quad (38)$$

where $r_{r,n}$ denotes the reference yaw rate at the nth time step and $F_{yf\_\max}$ and $F_{yr\_\max}$ represent the maximum lateral front and rear axle forces, respectively. $F_{yf\_\max}$ and $F_{yr\_\max}$ can be obtained using the tire model (21) and (22). Since $F_{yf\_\max}$ and $F_{yr\_\max}$ are dependent on μ and κ_i, $r_{r,n}$ can be appropriately restrained based on the surface conditions and the friction ellipse effect.

Operational Principal for Supervisor

The primary coordination of ESC and AFS is performed in the supervisor based on a rule-based algorithm presented in Alg. 1. This algorithm determines the values of τ_*, Q, and P and whether β_r has to be tracked or not in formulating the MPC problem to generate M_z. In Alg. 1, $\alpha_{f,p}$ and $\alpha_{r,p}$ are the peak front and rear slip angles that correspond with $F_{yf\_\max}$

Algorithm 1 Operational principal for supervisor

---

if $|\alpha_f| < |\alpha_{f,p}|$ and $|\alpha_r| < |\alpha_{r,p}|$ **then**

    $\tau_* = \tau_s$

    $Q\ \&\ P = G \cdot \mathrm{diag}\,[0,0,1,0,0]$

    Calulation of M_z using MPC with r_d

    if $|M_z| > |M_{z\_max,s}|$ **then**

        $M_z = M_z - M_{z\_max,s}$

        $\Delta\delta_f = \alpha_{f,p} - \alpha_f$

            ▷ AFS generates $M_{z\_max,s}$ while ESC creates M_z

    else

        $M_z = 0$

        Calculation of $\Delta\delta_f$ corresponding with M_z

        ▷ AFS solely generates M_z while ESC is deactivated

    end if

else

    $\tau_* = \tau_b$

    $Q\ \&\ P = G \cdot \mathrm{diag}\,[5,0,1,0,0]$

    Calulation of M_z using MPC with r_r, β_r, and M_{z_r}

    if $|\alpha_f| > |\alpha_{f,p}|$ **then**

        $\Delta\delta_f = \alpha_{f,p} - \alpha_f$

    end if

end if

---

and $F_{yr\_\max}$, respectively, $M_{z\_max,s}$ the maximum corrective yaw moment that can be generated by AFS, G a constant gain whose value is 1.5×10^8. As suggested in Alg. 1, before F_{yf} or F_{yr} are saturated, *i.e.* $|\alpha_f| < |\alpha_{f,p}|$ and $|\alpha_r| < |\alpha_{r,p}|$, the MPC problem is formulated to generate M_z with $\tau_* = \tau_s$ and $Q\ \&\ P = G \cdot \mathrm{diag}\,[0,0,1,0,0]$. When $|M_z| < |M_{z\_max,s}|$, AFS solely operates to recreate the generated M_z from the MPC problem to control the vehicle to follow only r_d as follows:

$$M_z = l_f \cdot \Delta F_{yf}(\Delta\delta_f), \quad (39)$$

where $\Delta F_{yf}(\Delta\delta_f)$ is the modified front lateral force, which is a function of $\Delta\delta_f$, by the AFS. Once $|M_z|$ becomes larger than $|M_{z\_max,s}|$, AFS is controlled to generate $M_{z\_max,s}$ by letting $\Delta\delta_f = \alpha_{f,p} - \alpha_f$ while ESC is activated to generate $M_z - M_{z\_max,s}$. When F_{yf} or F_{yr} is saturated, *i.e.* $|\alpha_f| > |\alpha_{f,p}|$ or $|\alpha_r| > |\alpha_{r,p}|$, ESC and AFS cooperate to control the vehicle to follow not only r_r but also the reference side slip angle, β_r with reference corrective yaw moment, M_{z_r}. Either the vehicle oversteers or understeers when $|\alpha_f| > |\alpha_{f,p}|$, AFS always control α_f not to exceed $\alpha_{f,p}$. The methods of generaing β_r and M_{z_r} are illustrated in the following subsections.

Generations of β_r and M_{z_r} for Understeering Vehicle

As seen in the first figure of Fig. 4a, when F_{yf} is saturated first, *i.e.* the vehicle understeers, ESC is activated to enlarge

(a)   (b)
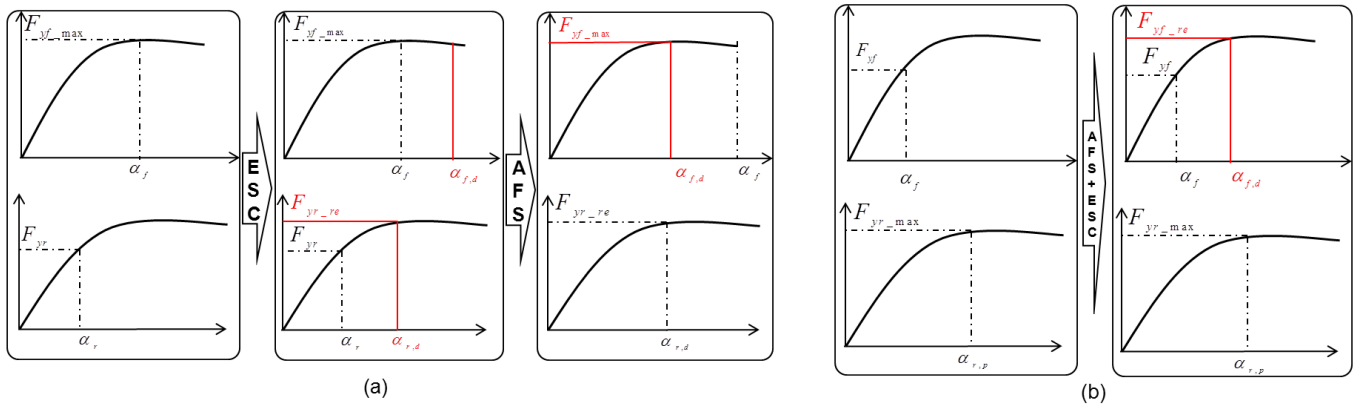
Figure 4. Procedures of coordinating ESC and AFS. (a) Understeering. (b) Oversteering.

the absolute value of β to increase the absolute value of α_r which is followed by increasing F_{yr}. To turn a vehicle at a steady state, the sum of the front and rear lateral forces have to be equal to the centrifugal force that is exerted on the mass center of gravity of the vehicle. Since the centrifugal force can be expressed as $mv_x r$, the required rear lateral force, F_{yf_re}, to turn the vehicle to track r_r at a steady state can be expressed as follows:

$$F_{yr\_re} = mv_x r_r - F_{yf\_\max}. \tag{40}$$

The value of α_r that corresponds with F_{yr_re} is the value of the desired rear side slip angle, $\alpha_{r,d}$. β_d can be obtained as follows:

$$\beta_r = \alpha_{r,r} + \frac{l_r \cdot r_r}{v_x}.$$

Since β affects both α_f and α_r according to (5) and (6), α_f moves to $\alpha_{f,e}$ with β_d, as seen in the second figure of Fig. 4a. Since α_f becomes unnecessarily large, AFS is activated to keep α_f near $\alpha_{f,p}$ as follows:

$$\Delta \delta_f = \alpha_{f,p} - \alpha_f.$$

At the state indicated by the first figure of Fig. 4a, the vehicle understeers at a steady state when the yaw moment balance is maintained, *i.e.* , $\dot{r} = 0$. Due to the activation of ESC, $F_y r$ grows to $F_{yr\, re}$. Consequently, the yaw moment balance is not kept at the state indicated by the second figure of Fig. 4a. To balance it again, reference corrective yaw moment M_{z_d} is defined as follows:

$$M_{z\_r} = -l_f F_{yf} + l_r F_{yr\_re}.$$

Generations of β_r and M_{z_r} For Oversteering Vehicle

At the state seen in the first figure of Fig. 4b, the yaw moment balance of the vehicle is kept with the saturated F_{yr}. When there is an additional steering input from the driver, instability of the vehicle can be caused due to the broken moment balance as F_{yf} grows. ESC initiates to keep the moment balance by generating M_z, although F_{yf} continues growing up to F_{yf_max}. The reference corrective yaw moment in this case is defined as follows:

$$M_{z\_r} = -l_f F_{yf\_re} + l_r F_{yr},$$

where

$$F_{yf\_re} = mv_x r_r - F_{yr\_\max}.$$

When the vehicle oversteers, AFS starts to operate when $\alpha_f > \alpha_{f,p}$ to keep α_f near $\alpha_{f,p}$ as follows:

$$\Delta \delta_f = \alpha_{f,p} - \alpha_f.$$

β_d is generated to keep α_r near $\alpha_{r,p}$ as follows:

$$\beta_r = \alpha_{r,p} + \frac{l_r \cdot r_r}{v_x}.$$

Coordinator for Optimal Distribution of Brake Forces

The coordinator that optimally distributes the brake forces to recreate the corrective yaw moment, M_z from the supervisor is built based on the coordinator that is introduced in (25).

The values of corrective yaw moments when exerting brake forces on the front, M_{zf} and on the rear, M_{zr} can be expressed as follows:

$$M_{zf} = \sin \delta_f \cdot l_f \cdot \Delta F_{yf} + \cos \delta_f \cdot t \cdot \Delta F_{xf}$$
$$M_{zr} = t \cdot \Delta F_{xr} - l_r \cdot \Delta F_{yr}.$$

ΔF_{x*} and ΔF_{y*} are the variations of the longitudinal force and the lateral force, respectively, when applying brake forces on the front or on the rear wheel. ΔF_{y*} at the current α_i with the varying κ_i can be calculated using the tire model (21) and (22). For optimal distribution of the brake forces, a cost function is defined as follows:

$$J_M(\Delta F_{xf}, \Delta F_{xr}) = |\Delta F_{xf}| + |\Delta F_{xr}| \tag{41}$$
$$\text{subj. to} \quad M_z = M_{zf} + M_{zr}. \tag{42}$$

Newton-Raphson method can obtain the optimal solution, ΔF_{xf}^* and ΔF_{xr}^*, that minimizes the cost function (41) while satisfying the equality constraint (42) at each time step. The brake pressure, which can create ΔF_{xf}^* and ΔF_{xr}^* at the given slip angle and slip ratio are calculated using the following equations:

$$P_{B*} = \frac{\Delta F_{x*}^*}{K_{B*}}, \tag{43}$$

where P_{B*} and K_{B*} denote the required cylinder brake pressure and the brake gain of the corresponding wheel, respectively.
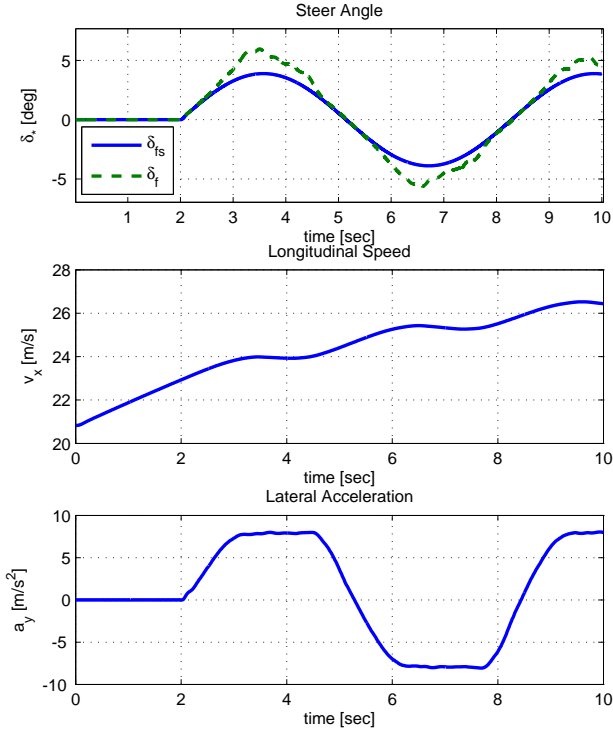
Figure 5. Vehicle maneuver on a high-μ surface ($\mu = 0.85$)

Simulation Results and Discussion

The performance of the proposed MPC-based algorithm that coordinates ESC and AFS was evaluated by simulations using the front wheel driving D-class sedan model in Carsim software.
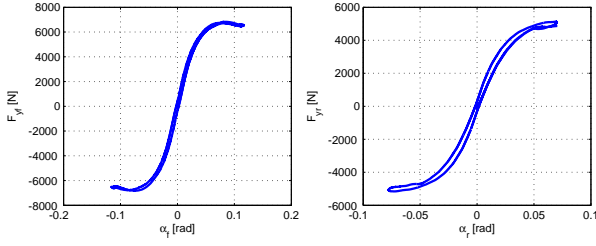
Simulation on a high-μ surface

In the first simulation, with the vehicle maneuver shown in Fig. 5, whose results are presented in Figs. 6-7, the verification of the proposed algorithm was carried out in a simulation environment on a high-μ surface with $\mu = 0.85$. The open loop slalom test with a 4 [deg] maximum front steer angle was performed to recreate the harsh simulation scenario. The proposed method successfully tracked the desired yaw rate while limiting the absolute value of β within certain boundary, as presented in the first and third plots in Fig. 6. As indicated in the second plot of Fig. 6, the dotted green line indicates M_z and the blue solid line represents the value of the corrective moment recreated by differential braking. The values of β_r are generated at each time step as in the fourth plot of Fig. 6. When AFS and ESC cooperate, a considerable amount of M_z can be recreated by AFS. When AFS cannot solely generate M_z, the yaw moment from the differential braking begins to be exerted. The fifth plot in Fig. 6 shows that the AFS successfully controls the front steer angle so that the value of α_f was kept near $\alpha_{f,p}$ to generate F_{yf_max} at the limit of handling. Since β_r is also tracked to make full use of the physical capacity of F_{yr}, the value of α_r also closely approaches to the value of $\alpha_{r,p}$. The values of P_B from the coordinator are plotted in the last plot of Fig. 6. As seen in the tire force curves presented in Fig.7, F_{yf} and
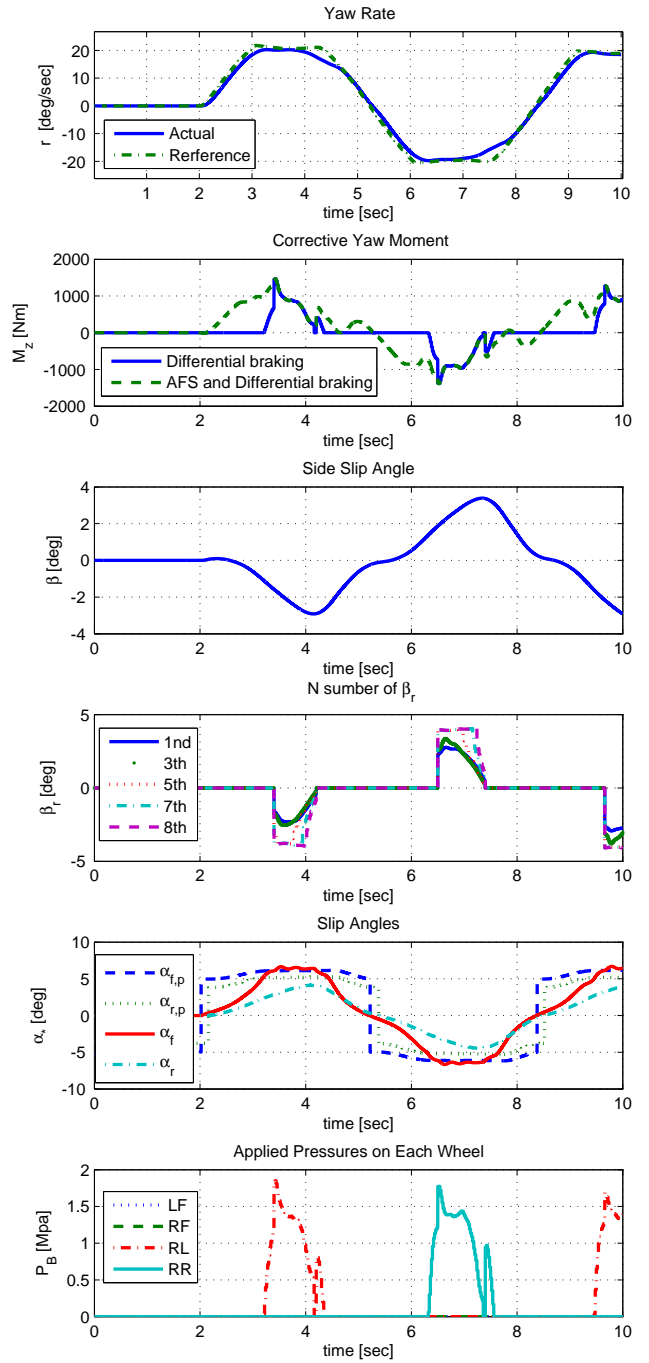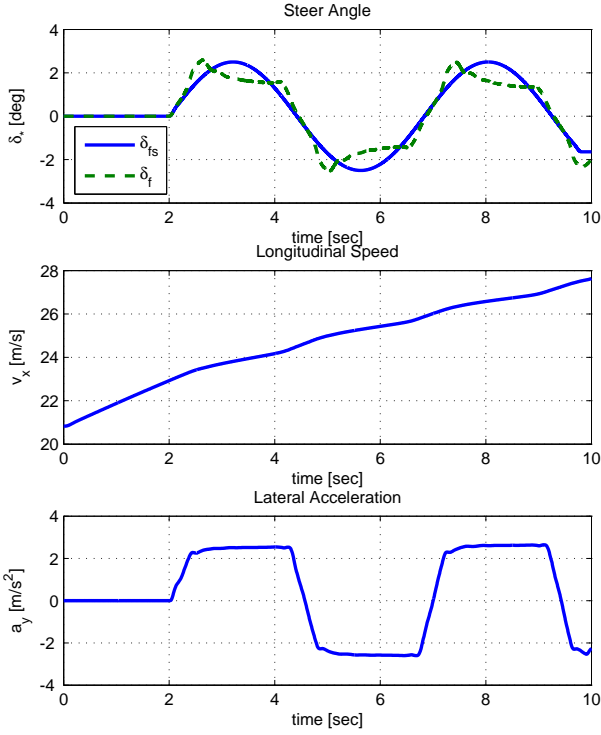

Figure 6. Control inputs and vehicle states on a high-μ surface ($\mu = 0.85$)

F_{yr} are bounded to have their maximum values. The steering input from the driver and its sum with modified steer angle from AFS is shown in Fig. 5.
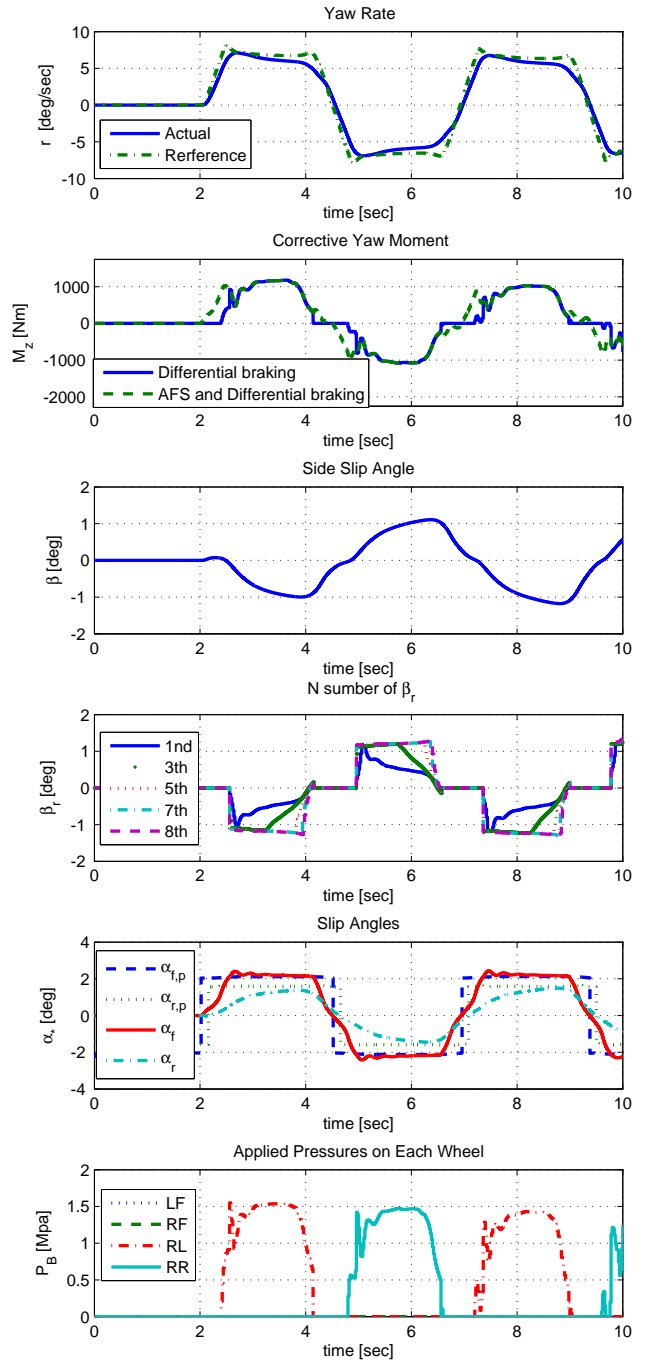
Figure 7. Tire force curves on a high-μ surface ($\mu = 0.85$)

Figure 8. Vehicle maneuver on a low-μ surface ($\mu = 0.3$)

Figure 9. Control inputs and vehicle states on a low-μ surface ($\mu = 0.3$)

Simulation on a low-μ surface

To validate the effectiveness of the proposed method on a low-μ surface, the simulation with the maneuver shown in Fig. 8 was performed on a low-μ surface with $\mu = 0.3$. Although the majority of the required M_z is recreated by differential braking on a low-μ surface, AFS can still generate some M_z and control the front steer angle to keep α_f near $\alpha_{f,p}$ at the limit of handling as seen in the second and fifth plots of Fig. 9. The proposed method successfully follows the desired yaw rate while keeping the absolute value of β within a certain boundary, as presented in the first and third plots in Fig. 9. The values of β_r are generated at each time step, as in the fourth plot of Fig. 9. As seen in the fifth plot of Fig. 9, when excessive front steer input from the driver is detected, AFS works to compensate the steer input. The values of P_B from the coordinator are plotted in the last plot of Fig. 9. As seen in Fig. 10, the lateral tire forces are generated close to their saturated values to turn the vehicle to its limit.
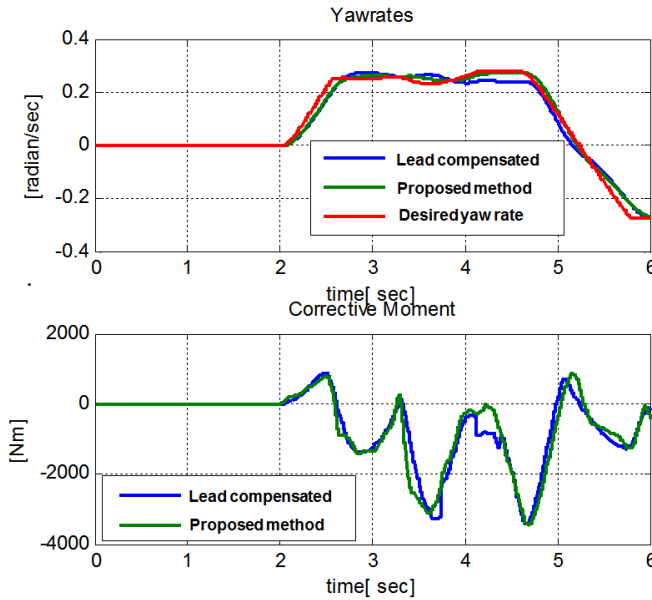
Comparison with lead compensator

By accounting for the lagged model of the actuator as shown in (13) in the prediction model, the supervisor can initiate early actuations to compensate the lagged characteristic of the actuator. It is worthwhile to compare this with a lead compensator since a lead compensator also enables the
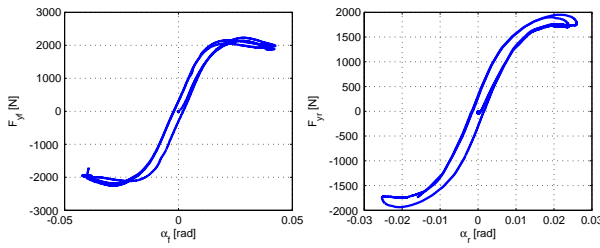
Figure 10. Tire force curves on a low-μ surface ($\mu = 0.3$)

Figure 11. Comparison with a lead compensator.

early actuation to minimize the deterioration of the control performance due to the late actuations. As seen in Fig. 11, the yaw rate from the vehicle controlled by the lead compensator has a larger deviation from the desired trajectory than that of the proposed method that initiate the early actuations based on models. The absolute value of the exerted moment to the vehicle from the lead compensator is also larger than the proposed method. The exerted moment from the lead compensator has some oscillations that even worsen the ride and handling performances of the vehicle. To conclude, by simply lead compensating the control input, the desired performance that is achieved by using MPC scheme is not guaranteed.

Conclusion

A novel method of coordinating ESC and AFS based on MPC has been developed and investigated in Carsim simulation environment. The proposed algorithm distinguishes itself from the previously reported methods by the following features: 1) it can reflect the lagged characteristics of lateral tire forces and actuators on the prediction model in the MPC formulation to better predict the vehicle behaviour; 2) it generates the desired values of side slip angle and corrective yaw moment to maintain the vehicle yaw stability while driving the vehicle as the driver intends; 3) a closed-form solution for the MPC problem with a reference state and inputs is obtained without requiring iterations of numeric

solvers and 4) it optimally allocates the modified front steer angle and the brake forces considering the friction ellipse effect with the current vehicle state and vertical loads. The simulation results of the suggested algorithm show that the suggested method can control the vehicle to track the reference states with minimum control inputs both on a high- and low-μ surfaces.

References

[1] K. Park, J. Lee, and J. Park, 'Torque control of a vehicle with electronic throttle control using an input shaping method," *IJAT*, vol. 14, no. 2, pp. 189–194, 2013.

[2] K. Nam, H. Fujimoto, and Y. Hori, 'Dynamic sensor zeroing algorithm of 6D IMU mounted on ground vehicles," *IJAT*, vol. 14, no. 2, pp. 221–231, 2013.

[3] J. Kim, and Y. Kim, 'Evelopment of active front wheel steering control system keeping stable region in driving phase diagram ," *IJAT*, vol. 15, no. 7, pp. 1107–1117, 2014.

[4] Y. H. Xu, and M. Ahmadian, 'Study on the performance of active front steering system ," *IJAT*, vol. 14, no. 4, pp. 595–603, 2013.

[5] D. Zhang, Q. Xiao and K. Li , "Driver curve speed model and its application to acc speed control in curved roads," *IJAT*, vol. 14, no. 2, pp. 241–247, 2013.

[6] X. Wang, S. Shi, L. Liu and L. Jin, "Analysis of driving mode effect on vehicle stabilitye," *IJAT*, vol. 14, no. 3, pp. 363-373, 2013.

[7] S. Kim, K. Park, H. Song, Y. Hwang, S. Moon, H. Ahn, and M. Tomizuka, "Study on the performance of active front steering system," *IJAT*, vol. 14, no. 4, pp. 595-603, 2013.

[8] J. Youn, "Heuristic resource allocation and scheduling method for distributed automotive control systems" *IJAT*, vol. 14, no. 4, pp. 611–624, 2013.

[9] R. Tchamna and I. Youn, "yaw rate and side-slip control considering vehicle longitudinal dynamics," *IJAT*, vol. 14, no. 1, pp. 53–60, 2013.

[10] B. S., "Cooperative lateral vehicle control for autonomous valet parking," *IJAT*, vol. 14, no. 4, pp. 633–640, 2013.

[11] S. A. Oleksowicz, "Investigation of regenerative and anti-lock braking interaction," *IJAT*, vol. 14, no. 4, pp. 641–650, 2013.

[12] H. S. Yoon, "Measurement of roof deformation caused by vehicle rollover," *IJAT*, vol. 14, no. 4, pp. 667–674, 2013.

[13] I. Kim, H. Kim, J. Bang, and K. Huh, "Development of estimation algorithms for vehicles mass and road grade," *IJAT*, vol. 14, no. 6, pp. 889–895, 2013.

[14] W. Z. Zhao, Y. J. Li, C. Y Wang, Z. Q. Zhang, and C. L. Xu, "Research on control strategy for differential steering system

based on h mixed sensitivity," *IJAT*, vol. 14, no. 6, pp. 913–919, 2013.

[15] J. D. and, "Preliminary results analyzing the effectiveness of electronic stability control (esc) systems," U.S. Department of Transportation," NHTSA Technical Report, 2004.

[16] M. Nagai, M. Shino, and F. Gao, "Study on integrated control of active front steer angle and direct yaw moment," *JSAE Review*, vol. 23, no. 3, pp. 309–315, July 2002.

[17] P. Falcone, F. Borrelli, J. Asgari, H. E. Tseng, and D. Hrovat, "Predictive active steering control for autonomous vehicle systems," *IEEE Trans. Contr. Syst. Technol.*, vol. 15, no. 3, pp. 566 – 580, 2007.

[18] C. E. Beal and J. C. Gerdes, "Model predictive contro for vehicle stabilization at the limits of handling," *IEEE Trans. Contr. Syst. Technol.*, vol. 21, no. 4, pp. 1258 – 1269, 2012.

[19] D. Bernardini, S. D. Cairano, A. Bemporad, and H. Tseng, "Drive by-wire vehicle stabilization and yaw regulation: A hybrid model predictive control design," in *Proc. 48th IEEE Conf. Descision and Control*, Shanghai, China, 2009, pp. 7621-7626.

[20] G. Palmieri, O. Barbarisi, S. Scala, and L. Glielmo, "A preliminary study to integrate ltv-mpc lateral vehicle dynamics control with a slip control," in *Proc. 48th IEEE Conf. Descision and Control*, Shanghai, China, 2009, pp. 4625-4630.

[21] P. Falcone, H. E. Tseng, F. Borrelli, J. Asgari, and D. Hrovat, "Mpc-based yaw and lateral stabilisation via active front steering and braking," *Veh. Syst. Dyn.*, vol. 46, pp. 611–628, 2008.

[22] S. D. Cairano, H. E. Tseng, D. Bernardini, and A. Bemporad, "Vehicle yaw stability control by coordinated active front steering and differential braking in the tire sideslip angles domian," *IEEE TCS*, vol. 21, no. 4, July 2013.

[23] J. Oh and S. Choi, "Vehicle velocity observer design using 6d imu and multiple observer approach," *IEEE Trans. Intell. Transport. Syst.*, vol. 13, no. 4, pp. 1865–1879, 2012.

[24] M. Choi, J. Oh, and S. B. Choi, "Linearized recursive least square methods for real-time identification of tire-road friction coefficient," *IEEE Trans. Veh. Technol.*, Vol.62, Issue 8, 2013.

[25] M. Choi, and S. B. Choi, "Model predictive control for vehicle yaw stability with practical concerns ," *IEEE Trans. Veh. Technol.*, Vol.63, Issue 8, 2014. .

[26] H. B. Pacejka, *Tire and Vehicle Dynamics*, 2nd ed. SAE, 2006.

[27] Y. Hsu, "Estimation and control of lateral tire forces using steering torque," Ph.D. dissertation, Stanford Univ., Stanford, CA, 2009.